IOPscience iopscience.iop.org

Home Search Collections Journals About Contact us My IOPscience

ZnO-based interdigitated MSM and MISIM ultraviolet photodetectors

This article has been downloaded from IOPscience. Please scroll down to see the full text article.

2010 J. Phys. D: Appl. Phys. 43 415103

(http://iopscience.iop.org/0022-3727/43/41/415103)

View the table of contents for this issue, or go to the journal homepage for more

Download details:
IP Address: 130.209.6.41
The article was downloaded on 05/04/2012 at 18:06

Please note that terms and conditions apply.

J. Phys. D: Appl. Phys. **43** (2010) 415103 (8pp) doi:10.1088/0022-3727/43/41/415103

ZnO-based interdigitated MSM and MISIM ultraviolet photodetectors

Ghusoon M Ali and P Chakrabarti

Center for Research in Microelectronics, Department of Electronics Engineering, Institute of Technology, Banaras Hindu University, Varanasi-221005, India

Received 29 March 2010, in final form 27 August 2010
Published 29 September 2010
Online at stacks.iop.org/JPhysD/43/415103

Abstract
The paper reports the fabrication and characterization of ZnO-based interdigitated metal–semiconductor–metal (MSM) and metal–insulator–semiconductor–insulator–metal (MISIM) ultraviolet photodetectors. The ZnO thin film was grown on a p-type Si ⟨1 0 0⟩ substrate by the sol–gel technique. With applied voltage in the range from −3 to 3 V we estimated the contrast ratio, responsivity, detectivity and quantum efficiency of the photodetectors for an incident optical power of 0.1 mW at 365 nm ultraviolet wavelength. The I–V characteristics were studied and the parameters such as ideality factor, leakage current and barrier height were extracted from the measured data. For Au/Cr/SiO_2/ZnO/ SiO_2/Al (MISIM) structure the product ($m\chi$) of the tunnelling effective electron mass (m) and the mean tunnelling barrier height (χ) was also extracted.

(Some figures in this article are in colour only in the electronic version)

1. Introduction

Ultraviolet (UV) detectors find applications in missile warning systems, UV astronomy, ozone layer monitoring, high-temperature flame and fire detection and environmental monitoring. ZnO, a promising environmentally friendly material, is widely deployed in the fabrication of UV photodetectors. The material has wide direct bandgap (3.37 eV at 300 K), high exciton binding energy (60 meV), excellent radiation hardness and large photoresponse. This material is inherently n-type because of the non-stoichiometry created by the presence of native donor defects, hydrogen defects, oxygen vacancies and/or zinc interstitials. ZnO thin-film-based UV photodetectors in the metal–semiconductor–metal (MSM) and metal–insulator–semiconductor–insulator–metal (MISIM) structure in the Schottky form have been investigated for fast response speed, easy fabrication and planar outlay. Good quality p–n junction photodetectors based on ZnO are difficult to fabricate because of the constraints associated with the growth of p-type ZnO [1–5].

Numerous research papers have reported ZnO-based Schottky diodes for UV detection. Jiang *et al* [6] reported an Au Schottky type ZnO MSM UV detector. ZnO film was obtained by the rf magnetron sputtering method. The detector exhibited a peak responsivity of 0.337 A W^{-1} at 360 nm. A Ag/ZnO Schottky contact fabricated by the pulsed laser deposition (PLD) method was reported by Li *et al* [5]. The device measured photocurrent-to-dark current ratios of 140.4 and 138.4 at a bias voltage of 5 V before and after annealing, respectively. Liang *et al* [7] reported ZnO Schottky UV photodetectors with MSM configuration using ZnO films grown by metalorganic chemical vapour deposition (MOCVD). The device exhibited a photoresponsivity of 1.5 A W^{-1}. Lin *et al* [8] reported an MSM based on Ru Schottky contact on ZnO films grown on sapphire substrates by molecular beam epitaxy (MBE). The extracted photocurrent-to-dark current contrast ratio is reported to be 225. Chen *et al* [9] reported an MSM with IrO_2 Schottky contact on ZnO thin films grown by the sol–gel method. The photocurrent was 2 orders of magnitude larger than the dark current. For a light wavelength of 360 nm and 5 V applied bias, the response was measured to be 0.011 A W^{-1}. Young *et al* [10] have examined ZnO thin-film-based MSM and MISIM photodetectors grown on sapphire substrates by MBE. It is demonstrated that ZnO-based MISIM photodetectors exhibit smaller dark current, larger photocurrent-to-dark current contrast ratio and larger UV-to-visible rejection ratio as compared with its MSM counterpart.

In this study we report the fabrication and characterization of Au/Cr Schottky contacts on ZnO thin films grown on p-type Si ⟨1 0 0⟩ substrates in the form of interdigitated MSM and MISIM structures. The ZnO film was obtained by the sol–gel

 © 2010 IOP Publishing Ltd Printed in the UK & the USA

method. The Au/Cr contact was deposited by a radio frequency (RF) sputtering deposition technique. The devices were tested to explore their potential as UV photodetectors.

2. Experiment

2.1. Preparation of ZnO thin film

The deposition of undoped ZnO thin film was carried out using the sol–gel technique. The substrate used for deposition is a p-Si ⟨1 0 0⟩ (≈380 μm thick) of resistivity 2–7 Ω cm. Before deposition of the ZnO film over Si, the substrate was cleaned by RCA-1 and RCA-2 aqueous cleaning processes. In RCA-1 procedure the cleaning agent consists of 5 parts deionized (DI) water, 1 part 27% ammonium hydroxide and 1 part 30% hydrogen peroxide while RCA-2 cleaning mixture makes use of 6 parts DI water, 1 part 27% hydrochloric acid and 1 part 30% hydrogen peroxide. Cleaning is followed by quenching of wafer in 10 parts DI water and 1 part hydrofluoric acid. RCA-1 is used as a procedure for removing organic residues and certain metals while RCA-2 is used for removing atomic and ionic contaminants. Quenching in 10 parts of DI water and 1 part of HF is used for stripping the oxide. The DI water (resistivity ∼18 MΩ cm) was obtained from the DI water plant of Millipore, India make (Model Milli-Q). Finally, the substrate was dried using dry nitrogen.

In the sol–gel technique, we used zinc acetate dihydrate which is well known as a starting material for the preparation of ZnO sols for coatings. This is a cheap material and has good solubility as compared with alkoxides like zinc-*n*-propoxide in alcohols. However, zinc acetate dihydrate has only limited solubility in alcohols in the absence of other agents or heating. In this work 2.19 g of zinc acetate dihydrate ($Zn(CH_3COO)_2 \cdot 2H_2O : ZnAc_2 \cdot 2H_2O$) was dissolved in 20 ml isopropanol ($(CH_3)_2CHOH$) and 0.8 g diethanolamine (DEA: $[CH_2(OH) \cdot CH_2]_2NH$) solution at room temperature. The DEA to zinc acetate molar ratio was kept as 1 : 1. After 1 h of stirring at room temperature, a transparent sol–gel was obtained. The resultant solution thus prepared was subsequently used for coating. The films were prepared by spin-coating the sol–gel on the wafers for 10 s at a speed of 1000 rpm followed by a spin for 40 s at a speed of 4000 rpm. This step was followed by preheating the coating at 100 °C for 10 min on a hot plate and post-heating at 450 °C for 1 h [11, 12].

An array of four interdigitated electrode patterns was created on the sample (size 1 cm × 1.5 cm). Each pattern consists of 10 fingers with a length of 500 μm and width (w) of 40 μm with an inter-electrode spacing (s) of 60 μm. The pattern was spread over an active area of 1100 μm × 600 μm. Prior to direct writing on samples, the samples were post-cleaned by acetone and isopropanol and heated at 100 °C for 10 min to remove any trace of solvents. The photoresist AZ5214E was applied on the film using a spinner right after post-cleaning. The sample was baked for 50 s at 110 °C on a hot plate and subsequently exposed to UV radiation and post-baked for 1 min at 145 °C on the hot plate. For the MSM photodetector structure a set of interdigitated arrays was patterned and repeated throughout the wafer using a laser writer (model LW405 from MICROTECH: 405 nm gallium nitride diode writing laser). After direct laser writing, the pattern was developed in a MF26 developer for 50 s and the substrate was then rinsed in DI water and dried using nitrogen. Au/Cr (Au/Cr 100 nm/14 nm) metallization was carried out using an Anelva RF Sputtering System (model SPF-332H). Cr was used to improve the adhesion of the metal onto ZnO and a lift-off technique was used in the fabrication. For MISIM photodetectors, we first deposited 5 nm thick SiO_2 by the RF sputtering technique on ZnO/Si samples for the formation of an insulator layer. This step was subsequently followed by the same Au/Cr film deposition and lift-off technique. The schematic of the fabricated MSM and MISIM devices is shown in figure 1.

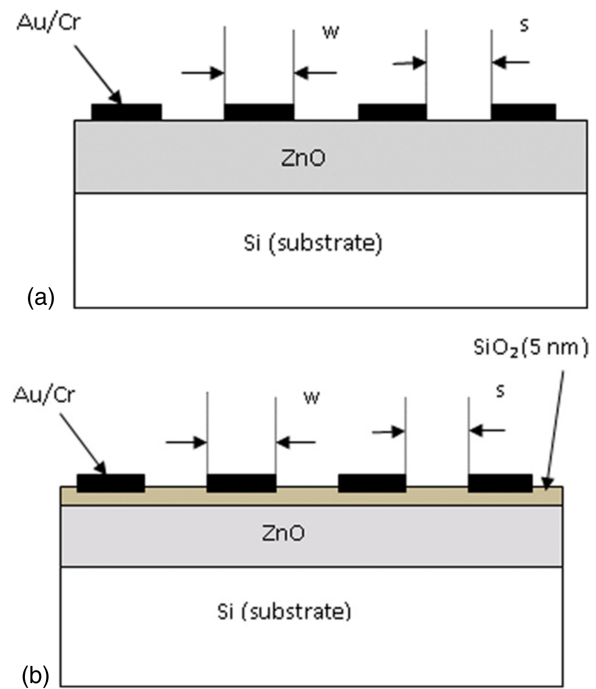

Figure 1. Structure of (*a*) MSM photodetector and (*b*) MISIM photodetector.

2.2. Characterization

The surface properties of the sample, such as the surface roughness and grain size, were measured using an atomic force microscope (AFM) of NT-MDT, Russia make (Model: PRO 47). The crystal structure of the ZnO films were characterized by x-ray diffraction (XRD) analysis using Cu Kα radiation in the range $2\theta = 20°–80°$. For studying the surface chemical bonding, x-ray photoelectron spectroscopy (XPS) measurements were performed using a VG Microtek ESCA 2000 with Mg Kα as the x-ray source. The obtained spectra were calibrated to a C1s electron peak at 285 eV. The absorbance spectra of the ZnO thin film were studied using a double beam spectrophotometer from Perkin-Elmer, Germany (model-Lambda 25), in the wavelength range from 200 to 1000 nm. The thickness of the ZnO film was measured by a Dektak Surface Profiler, USA.

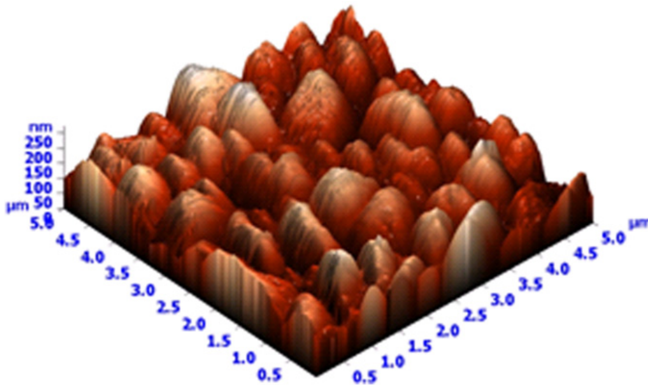

Figure 2. AFM 3D image of ZnO film on Si ⟨1 0 0⟩ substrate.

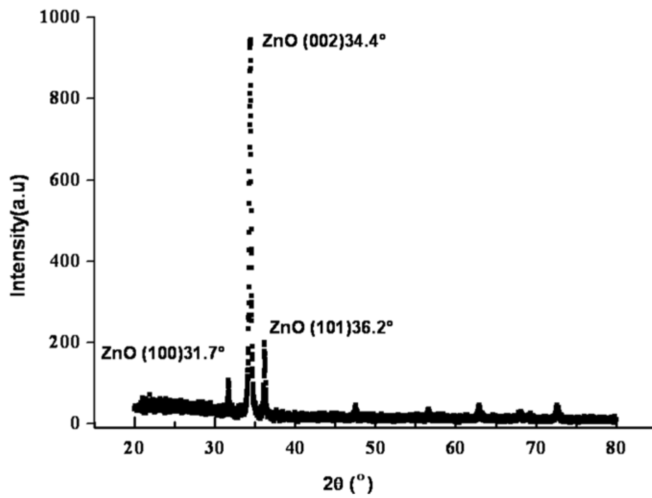

Figure 3. XRD pattern of the ZnO film.

The I–V characteristics were measured using an HP Semiconductor Parameter Analyzer (SPA) from Hewlett-Packard, USA (Model No 4145B), at room temperature (27 °C) for applied voltages ranging between −3 and +3 V under both dark and UV illumination. The optical characteristics were obtained using a UV lamp from BENCHMARK, India make, operating at 365 nm and an Optical power meter Model No FOMP-101 from BENCHMARK, India.

3. Results and discussion

The typical AFM 3D images of the prepared ZnO samples are shown in figure 2. The AFM images confirm that the ZnO films grown on Si substrates are polycrystalline in nature. The images also clearly demonstrate the formation of vertically well-aligned ZnO nanoneedle arrays with a good surface morphology. The XRD spectrum for the ZnO thin film prepared by sol–gel on the Si substrate presents an intense peak of (0 0 2) c-axis orientation of the wurtzite structure as can be seen from figure 3. The dominant peak in the XRD spectrum is at 34.4°. The diffraction peaks in figure 3 match the hexagonal ZnO structure with lattice constants of $a = 0.325$ nm and $c = 0.521$ nm [2, 12].

The crystallinity and microstructure of the films are essentially determined by the grain size. The grain size was found to depend on the post-deposition annealing temperature. The grain size was found to increase with increasing annealing temperature in the 350–600 °C range. An increase in the grain size causes the grain boundary density and carrier diffusion to decrease and mobility of charge carrier to increase [13, 14].

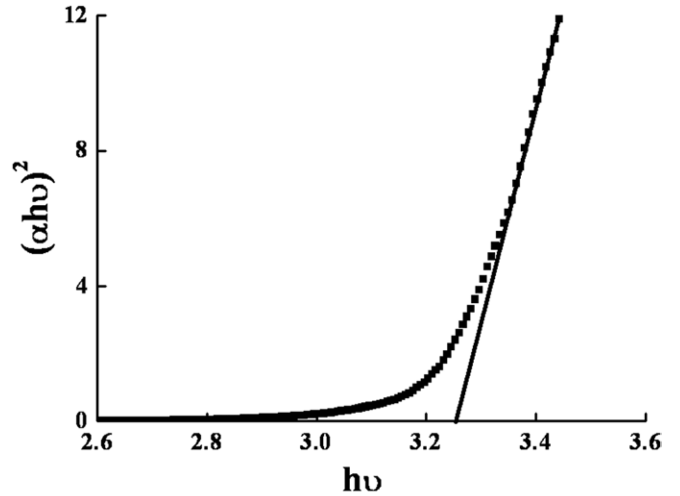

Figure 4. Variations of $(\alpha h\nu)^2$ versus $h\nu$ of the detector.

Furthermore, high temperature creates more defects such as oxygen vacancies which increase the value of carrier concentration [15]. The annealing temperature was set at 450 °C in this study. The root mean square (rms) value of roughness of the ZnO film deposited on the Si substrate annealed at 450 °C was measured to be 35 nm. The average grain size was measured to be 832 nm.

The thickness of the ZnO film was estimated to be in the range 125–150 nm as measured by the Dektak Surface Profiler. The bandgap of ZnO was evaluated from the absorbance spectra of the ZnO thin film using the double beam spectrophotometer in the wavelength range from 200 to 1000 nm. The optical bandgap of ZnO was estimated using the fundamental relation given by [6]

$$\alpha h\nu = B(h\nu - E_g)^n, \quad (1)$$

where α is the absorbance, $h\nu$ is the energy of absorbed light, $n = 1/2$ for direct allowed transition and B is the proportionality constant. The energy gap (E_g) was obtained by plotting $(\alpha h\nu)^2$ versus $h\nu$ and extrapolating the linear portion of $(\alpha h\nu)^2$ versus hν so as to cut the $h\nu$ axis as shown in figure 4.

The optical bandgap of ZnO was estimated to be 3.26 eV at 300 K. The absorption coefficient α_{coeff} was calculated from the absorbance α and the film thickness d using the following relation: [4]

$$\alpha_{coeff} = 2.303 \times \left(\frac{\alpha}{d}\right). \quad (2)$$

The absorption depth (penetration depth) δ_α is the reciprocal of absorption coefficient [16]. The penetration depth of UV light at 365 nm into ZnO prepared by the sol–gel method was found to be ~80 nm.

Figure 5 shows the core level XPS spectra of O1s for a typical ZnO thin film sample. The dominant peak comes from O–Zn bonds, namely lattice of the ZnO layer. The O1s is

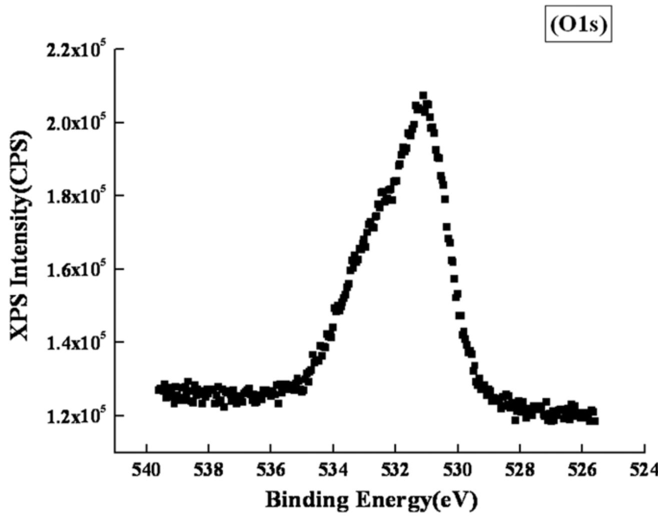

Figure 5. XPS O1s spectra of the ZnO thin film.

observed at about 531.1 eV, and corresponds to O^{2-} on the normal wurtzite structure of ZnO single crystal. A shoulder observed at the higher energy side than that of O–Zn bond is attributed to O–H bonds. Those O–H bonds are expected to exist on the surface since hydrogen atoms in ZnO are known to work as shallow donors [17, 18].

The basic MSM structure consists of two Schottky contacts, separated by a layer of semiconductor. A 5 nm SiO_2 layer below each Schottky contact is inserted to form the MISIM structure. In order to examine the effect of inserting an interfacial insulator layer on Schottky contact properties an Al electrode is deposited at a distance of 1 mm from the Schottky interdigitated electrodes for both devices to form an ohmic contact. Figure 6 shows the planar Schottky structure for both configurations.

Figure 7 shows the I–V characteristics measured in the dark for a single Schottky contact of MSM (Au/Cr/ZnO/Al) and MISIM (Au/Cr/SiO_2/ZnO/SiO_2/Al). Both devices apparently show rectifying behaviour. For the same applied voltage (forward or reverse) the current through the MISIM diode is found to be comparably less than that of the corresponding MSM configuration.

The current across a Schottky diode (without an insulating layer) is governed by thermionic emission theory given by [19]

$$I = \left[AA^*T^2 \exp\left(-\frac{q\phi_B}{kT}\right)\right]\left[\exp\left(\frac{qV}{nkT}\right) - 1\right], \quad (3)$$

where A is the Schottky contact area, A^* the effective Richardson constant (theoretically $A^* = 32 \times 10^4\ \mathrm{A\,m^{-2}\,K^{-2}}$ for ZnO using $m^* = 0.27m_o$) [19, 20], T the absolute temperature, q the charge of an electron, n the ideality factor, k the Boltzmann constant and ϕ_B the barrier height.

For a Schottky diode with an interfacial insulator layer, Card and Rhoderick [21] reported that current across MISIM is the same as equation (1) except for an additional exponential factor dependent on the interfacial layer parameter. The I–V relation for the insulated Schottky contact can be

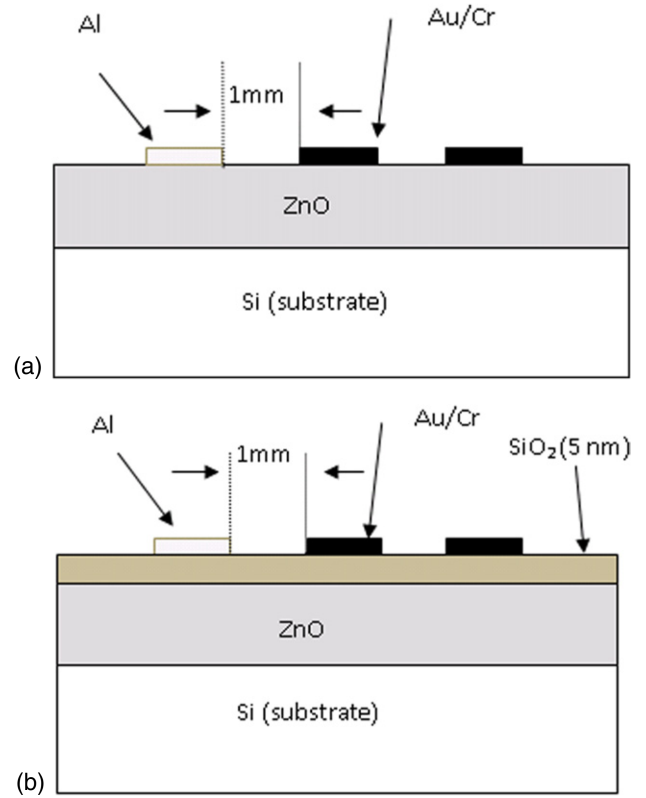

Figure 6. Structure of (*a*) planar Schottky diode and (*b*) planar MISIM Schottky diode.

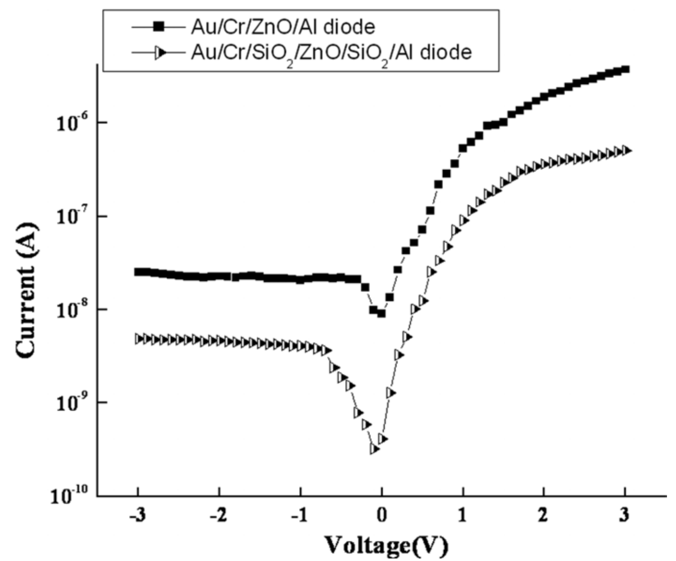

Figure 7. I–V characteristics of Au/Cr/ZnO/Al and Au/Cr/SiO_2/ZnO/SiO_2/Al Schottky contacts.

expressed as

$$I = \left[AA^*T^2 \exp\left(-\frac{q\phi_B}{kT}\right)\right]\left[\exp\left(\frac{qV}{nkT}\right) - 1\right] \times \left[\exp\left(\frac{4\pi\delta\sqrt{2m\chi}}{h}\right)\right], \quad (4)$$

where δ is the thickness of the insulating layer, χ is the mean tunnelling barrier height of the insulator layer, m and h are

Table 1. Device parameters.

Parameter	Au/Cr/ZnO/Al MSM structure	Au/Cr/SiO_2/ZnO/SiO_2/Al MISIM structure
Ideality factor	8	2.4
Turn on voltage (V)	0.6	0.4
Saturation current (A)	5×10^{-9}	1.5×10^{-10}
Barrier height (eV)	0.748	0.838

the tunnelling effective electron mass and Planck's constant, respectively.

The factor $\exp((4\pi\delta/h)\sqrt{(2m\chi)})$ corresponds to tunnelling probability and largely depends on the characteristics of the interfacial layer. This factor results in a depression of I–V characteristics when compared with the corresponding MSM configuration (without an insulating layer).

The values of barrier height, ideality factor, saturation current and turn-on voltage were extracted from the data of I–V characteristics of the Au/Cr/ZnO/Al contact. The value of the ideality factor was calculated from the slope of the $\ln(I)$ versus V plot (not shown here) in the voltage range 0.25–0.45 V. The value of ideality factor was estimated to be of the order of 8. The barrier height evaluated at room temperature (300 K) was found to be $\phi_B = 0.7480$ eV. The turn-on voltage was found to be 0.6 V and the saturation current $I_S = 5 \times 10^{-9}$ A.

From the data of I–V characteristics for the Au/Cr/SiO_2/ZnO/SiO_2/Al (MISIM) the saturation current was extracted and was found to be 1.5×10^{-10} A. The barrier height of MISIM ($\phi_{\text{B-MISIM}}$) with an interfacial insulator layer evaluated at room temperature (300 K) was found to be 0.838 eV. The larger value of barrier height is responsible for the lower saturation current in the case of insulated Schottky contact.

The value of ideality factor in this case was estimated to be 2.4. The turn-on voltage was found to be 0.4 V.

Table 1 summarizes the Schottky diode parameters for the two configurations (MSM and MISIM). It can be easily seen that inserting a 5 nm SiO_2 layer between the ZnO thin film and the Schottky contact enhances the barrier height, reduces the saturation current to one order and improves the ideality factor.

The insulating SiO_2 layer enhances the barrier height and reduces the thermal emission of electron along the barrier [22, 23]. The barrier height of MISIM with an interfacial insulator layer of thickness δ can be written as [24]

$$\phi_{\text{B-MIS}} = \phi_B + \Delta\phi, \tag{5}$$

$$\Delta\phi = \frac{4\pi kT\delta}{h}(2m\chi)^{1/2}, \tag{6}$$

where ϕ_B is the barrier height without the interfacial layer and $\Delta\phi$ is the additional barrier due to the insulator, χ is the mean tunnelling barrier height of the insulator layer, m and h are the tunneling effective electron mass and Planck's constant, respectively. From the above experimental measurement $\Delta\phi$ was found to be 0.092 eV.

Until now no values have been reported for the tunneling effective electron mass (m) and the mean tunnelling barrier height (χ) of the thin insulator layer for ZnO/SiO_2. From equations (5) and (6) we can extract the product of the tunnelling effective electron mass and mean tunnelling barrier height ($m\chi$) for ZnO/SiO_2. The extracted value of $m\chi$ is (4.1421×10^{-51} kg J $= 0.0284m_o$ eV) where m_0 is the rest mass of electron.

The devices were subsequently tested for their photoresponse in the ultraviolet region. When the incident photons are absorbed inside the ZnO thin film, electron–hole pairs are generated. The photogeneration is governed by desorption and adsorption of oxygen at the ZnO surface. In ZnO thin films it has been understood that the following trapping mechanism governs the photoresponse. Under dark conditions, oxygen is adsorbed by capturing a free electron from the surface of the n-type ZnO, which creates a depletion layer near the surface of the film which can decrease the film conductivity. The surface related process can be described as [2, 4]

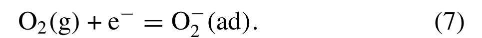

$$O_2(g) + e^- = O_2^-(ad). \tag{7}$$

Under UV illumination the electron–hole pairs are photogenerated:

$$h\nu \Rightarrow h^+ + e^-, \tag{8}$$

where h^+ and e^- represent electron and hole, respectively. Consequently, the photogenerated holes will be drifted by the electric field in the direction of the field extending the depletion layer. These carriers move towards the surface and neutralize the adsorbed oxygen which causes the surface conductivity to increase:

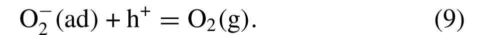

$$O_2^-(ad) + h^+ = O_2(g). \tag{9}$$

The hole-trapping mechanism through oxygen adsorption and desorption has been understood to be the dominant process in ZnO thin films [4]. The detector also showed response to visible light with lower sensitivity attributing to inherent defects in the ZnO film. Previous studies have indicated that intrinsic defects in ZnO films prepared by sol–gel, such as zinc vacancy V_{Zn}, oxygen vacancy V_O, interstitial zinc Zn_i, interstitial oxygen O_i and antisite oxygen O_Z, located above the valence band about 2–2.8 eV are responsible for the ZnO photoresponse in this range [25, 26].

Figure 8 shows the I–V characteristics measured in the dark and UV illumination (wavelength of 365 nm) with an optical power of 0.1 mW at room temperature for interdigitated MSM (Au/Cr/ZnO/Au/Cr) and MISIM (Au/Cr/SiO_2/ZnO/SiO_2/Al) photodetectors. It is seen that for a given applied voltage, there is a significant change in the current in the presence of UV radiation at 365 nm.

Contrast ratio is an important figure of merit of a UV detector. The contrast ratio (sensitivity) is defined as the ratio of the current under illumination to the dark current [10]. Figure 9 shows the dependence of the contrast ratio on the applied voltage for UV light at an optical power level of 0.1 mW for both MSM and MISIM structures.

In this study the contrast ratio (sensitivity) of MISIM was found to be much higher than that of MSM because of the significant reduction in dark current due to the presence of the SiO_2 layer. With 3 V applied bias, it was found that the measured dark currents were 5.63×10^{-7} A and 3.75×10^{-8} A for MSM and MISIM photodetectors, respectively. This is in

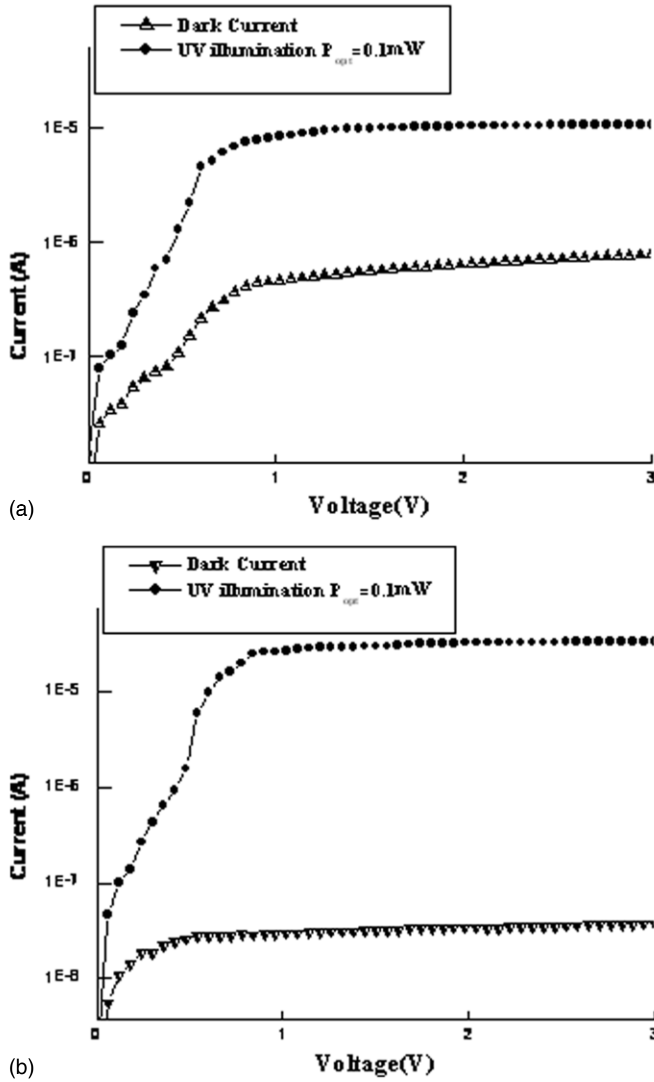

Figure 8. I–V characteristics of the fabricated photodetectors measured in dark and under UV illumination: (*a*) MSM (Au/Cr/ZnO/Cr/Au) and (*b*) MISIM (Au/Cr/SiO_2/ZnO/SiO_2/Cr/Au).

agreement with the result reported by Young *et al* [10]. It is further seen that the insertion of the 5 nm insulator layer significantly reduces the dark current but does not affect the current under illumination significantly. For this reason the sensitivity of the MISIM photodetector becomes higher than the MSM photodetector. The high contrast ratio (sensitivity) of the detector is due to the presence of oxygen-related hole-trap states at the thin films' surface as explained above, which prevents charge-carrier recombination and extends the holes' lifetime. Also the large surface-to-volume ratio in the nanostructure of ZnO thin films and the presence of deep level surface trap states make the lifetime of the photogenerated carriers longer [2, 6]. In fact, the combination of long lifetime and short transit time of charge carriers can result in a large difference between the current under illumination and dark current. The O/E conversion efficiency is measured by the quantum efficiency η and is given by [19]

$$\eta = \frac{I_{ph}}{P_{opt}} \times \frac{h\nu}{q}, \qquad (10)$$

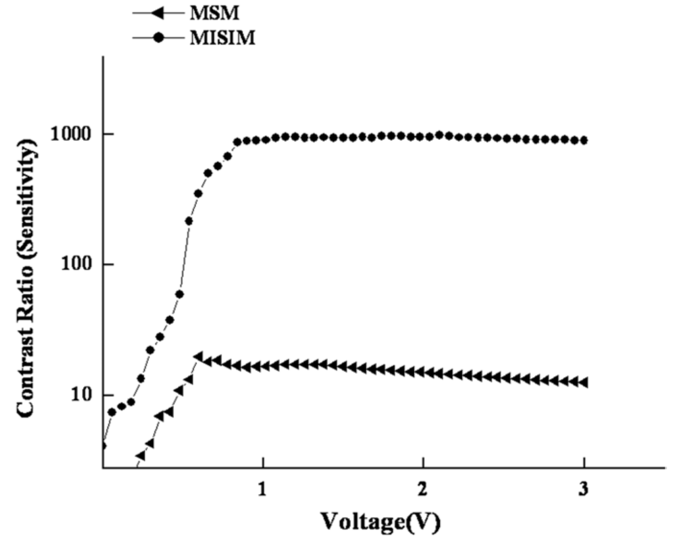

Figure 9. Variation of contrast ratio with applied voltage under UV illumination for MSM and MISIM structures.

where I_{ph} is the photocurrent, P_{opt} is the incident optical power, q is the electron charge, h is Planck's constant and ν is the frequency of light. It is observed that the MSM photodetector has a quantum efficiency of 19% for a bias voltage of 3 V under UV illumination. On the other hand for the MISIM photodetector, the quantum efficiency at the same voltage under UV illumination is approximately 70%. The responsivity R is given by [19]

$$R = \frac{q\lambda}{hc}. \qquad (11)$$

The responsivity values for MSM and MISIM at 3 V bias voltage for UV illumination (365 nm) are found to be 0.056 A W^{-1} and 0.206 A W^{-1}, respectively. The voltage dependent detectivity (D) of the device is given by [27]

$$D = \frac{\lambda\eta q}{hc}\left(\frac{RA}{4kT}\right)^{1/2}, \qquad (12)$$

where η is the internal quantum efficiency, k is the Boltzmann constant, T is the temperature and RA is resistance–area product of the device and can be obtained from the J–V characteristics as [19]

$$RA = \left(\frac{\partial J}{\partial V}\right)^{-1}. \qquad (13)$$

The variation of detectivity of the MSM and MISIM structures with the applied voltage is shown in figure 10. It can be easily seen that the detectivity of the photodetectors at an operating wavelength of 365 nm is more or less independent of the applied voltage. However, the detectivity of MISIM is nearly 4–5 times higher than the MSM counterpart. The values of zero bias resistance–area product (R_0A) are found to be 8.68 Ω m^2 and 16.50 Ω m^2 for the MSM and MISIM structures, respectively. The detectivity values (at zero bias) for the MSM and MISIM photodetectors are estimated to be 1.28×10^9 mHz$^{1/2}$ W^{-1} and 6.50×10^9 mHz$^{1/2}$ W^{-1}, respectively. A comparative performance rating of the two UV photodetector configurations is given in table 2.

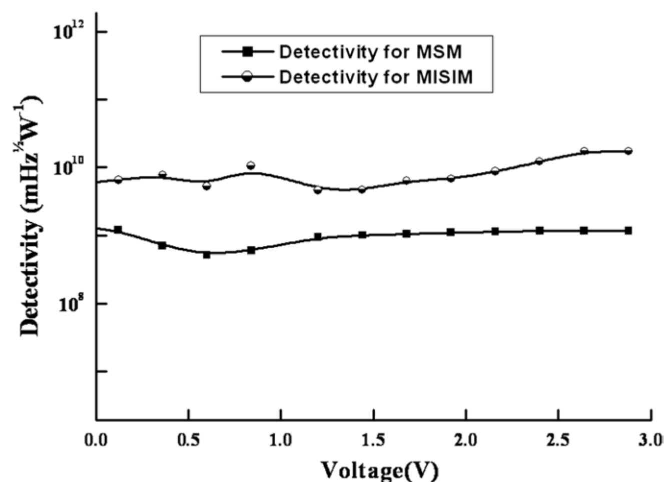

Figure 10. Variation of detectivity of MSM and MISIM photodetectors with applied voltage.

Table 2. Performance ratings of MSM and MISIM photodetectors.

Parameter	MSM photodetector	MISIM photodetector
Quantum efficiency (%)	19	70
Responsivity ($A\,W^{-1}$)	0.056	0.206
Contrast ratio (sensitivity)	12	904
Detectivity ($mHz^{1/2}\,W^{-1}$)	1.28×10^9	6.50×10^9
R_0A ($\Omega\,m^2$)	8.68	16.50

4. Conclusions

In this work, fabrication and characterization of interdigitated Schottky type MSM and MISIM photodetectors based on a ZnO thin film have been reported. The high quality ZnO thin film was obtained by the sol–gel technique. The photoresponse properties under UV illumination were studied at room temperature. It was found that by inserting a 5 nm insulator (SiO_2 in this case) just under the Schottky contact, the performance of the photodetector can be improved with respect to photocurrent, contrast ratio, dark current and detectivity. The devices are expected to find applications in photonic devices and systems as IC compatible photodetectors.

Acknowledgments

One of the authors Ms Ghusoon M Ali wishes to thank ICCR (Indian Council for Cultural Relations) for financial support under Indo-Iraq cultural exchange programme. The authors also thank the Indian Institute of Science, Bangalore, for extending the research facility under INUP programme.

References

[1] Özgür Ü, Alivov Y I, Liu C, Teke A, Reshchikov M A, Doğan S, Avrutin V, Cho S-J and Morkoç H 2005 A comprehensive review of ZnO materials and devices *J. Appl. Phys.* **98** 041301

[2] Ali G M, Singh S and Chakrabarti P 2009 Fabrication and characterization of ZnO photodetectors with high gain *J. Nanoelectrons Optoelectrons* **4** 316–20

[3] Angadi B, Park H C, Choi H W, Choi J W and Choi W K 2007 Oxygen plasma treated epitaxial ZnO thin films for Schottky ultraviolet detection *J. Phys. D: Appl. Phys.* **40** 1422–5

[4] Sharma P, Sreenivas K and Rao K V 2003 Analysis of ultraviolet photoconductivity in ZnO films prepared by unbalanced magnetron sputtering *J. Appl. Phys.* **93** 3963–70

[5] Li X, Li Q, Liang D and Xu Y 2009 Electrical properties of silver Schottky contacts to ZnO thin films *Optoelectron. Lett.* **5** 216–9

[6] Jiang D, Zhang J, Lu Y, Liu K, Zhao D, Zhang Z, Shen D and Fan X 2008 Ultraviolet Schottky detector based on epitaxial ZnO thin film *Solid-State Electron.* **52** 679–82

[7] Liang S, Sheng H, Liu Y, Huo Z, Lu Y and Shen H 2001 ZnO Schottky ultraviolet photodetectors *J. Cryst. Growth* **225** 110–3

[8] Lin T K, Chang S J, Su Y K, Huang B R, Fujita M and Horikoshi Y 2005 ZnO MSM photodetectors with Ru contact electrodes *J. Cryst. Growth* **281** 513–17

[9] Chen K J, Hung F Y, Chang S J and Young S J 2009 Optoelectronic characteristics of UV photodetector based on ZnO nanowire thin film *J. Alloys Compounds* **479** 674–7

[10] Young S J, Ji L W, Chang S J, Liang S H, Lam K T, Fang T H, Chen K J, Du X L and Xue Q K 2008 ZnO-based MIS photodetectors *Sensors Actuators* A **141** 225–9

[11] Habibi M H and Sardashti M K 2008 Structure and morphology of nanostructured zinc oxide thin films prepared by dip *vs.* spin-coating methods *J. Iran. Chem. Soc.* **5** 603–9

[12] Kamalasanan M N and Chandra S 1996 Sol–gel synthesis of ZnO thin films *Thin Solid Films* **288** 112–15

[13] Lee J, Yeo B and Park B 2004 Effects of the annealing treatment on electrical and optical properties of ZnO transparent conduction films by ultrasonic spraying pyrolysis *Thin Solid Films* **457** 333–7

[14] Ali G M, Dwivedi A D D, Singh S and Chakrabarti P 2010 Interface properties and junction behavior of Pd contact on ZnO thin film grown by vacuum deposition technique *Phys. Status Solidi* C **7** 252–5

[15] Zhu B L, Sun X H, Zhao X Z, Su F H, Li G H, Wu X G, Wu J, Wu R and Liu J 2008 The effects of substrate temperature on the structure and properties of ZnO films prepared by pulsed laser deposition *Vacuum* **82** 495–500

[16] Robertson V, Ward A, Low J and Reed A 2006 *Electrotherapy Explained: Principles and Practice* 4th edn (London: Elsevier)

[17] Ogata K, Komuro T, Hama K, Koike K, Sasa S, Inoue M and Yano M 2004 Control of chemical bonding of the ZnO surface grown by molecular beam epitaxy *Appl. Surf. Sci.* **237** 348–51

[18] Wei X Q, Man B Y, Liu M, Xue C S, Zhuang H Z and Yang C 2007 Blue luminescent centers and microstructural evaluation by XPS and Raman in ZnO thin films annealed in vacuum, N_2 and O_2 *Physica* B **388** 145–52

[19] Sze S M 1981 *Physics of Semiconductor Devices* 2nd edn (New York: Wiley)

[20] Allen M W, Alkaisi M M and Durbin S M 2006 Metal Schottky diodes on Zn-polar and O-polar bulk ZnO *Appl. Phys. Lett.* **89** 103520

[21] Card H C and Rhoderick E H 1971 Studies of tunnel MOS diodes: I. Interface effects in silicon Schottky diodes *J. Phys. D: Appl. Phys.* **4** 1589–601

[22] Jun Z J, Bo W, Lian J R, Xiang L C, Li J X, Li X Z, Jun C D, Ping H, Rong Z and Dou Z Y 2007 Photoresponse of the

In0.3Ga0.7N metal–insulator–semiconductor photodetectors *Chin. Phys.* **16** 2120–2

[23] Chand S and Bala S 2007 Simulation studies of current transport in metal–insulator–semiconductor Schottky barrier diodes *Physica* B **390** 179–84

[24] Bakker G W, Roulston D J and Eltoukhy A A 1984 Effective recombination velocity of polysilicon contacts for bipolar transistors *Electron. Lett.* **20** 622–4

[25] Zhang L, Yin L, Wang C, Lun N and Qi Y 2010 Sol–gel growth of hexagonal faceted ZnO prism quantum dots with polar surfaces for enhanced photocatalytic activity *Appl. Mater. Interfaces* **2** 1769–73

[26] Lan W, Peng X, Liu X, He Z and Wang Y 2007 Preparation and properties of ZnO thin films deposited by sol–gel technique *Front. Mater. Sci. China* **1** 88–91

[27] Chakrabarti P, Krier A and Morgan A F 2003 Analysis and simulation of a mid-infrared P^+-$InAs_{0.55}Sb_{0.15}P_{0.30}$/$n^0$-$InAs_{0.89}Sb_{0.11}$/$N^+$-$InAs_{0.55}Sb_{0.15}P_{0.30}$ double heterojunction photodetector grown by LPE *IEEE Trans. Electron Devices* **50** 2049–58